

Lifetime estimation of a covered overhead line conductor

Tapio Leskinen[†]

Ensto Utility Networks, POB 51, 06101 Porvoo, Finland

Kari Kantola[‡]

Helsinki University of Technology, POB 4300, 02015 HUT, Finland

(Received November 11, 2002, Accepted July 30, 2003)

Abstract. The paper presents results of studies concerning wind-induced aeolian vibration and fatigue of a 110 kV covered conductor overhead line. Self-damping measurement techniques are discussed: power method is found to be the most reliable technique. A method for compensating tension variations during the self-damping test is presented. Generally used empirical self-damping power models are enhanced and the different models are compared with each other. The Energy Balance Analysis (EBA) is used to calculate the aeolian vibration amplitudes, which thereafter are converted to bending stress for the calculation of conductor lifetime estimate. The results of EBA are compared with field measurements. Results indicate that adequate lifetime estimates are produced by EBA as well as field measurements. Generally the EBA gives more conservative lifetime expectancy. This is believed to result from the additional damping existing in true suspension structures not taken into account by EBA. Finally, the correctness of the line design is verified using Cigre's safe design tension approach.

Keywords: aeolian vibration; transmission line; conductor; lifetime; self-damping; energy balance principle.

1. Introduction

Transmission line conductors are subjected to various types of wind-induced excitation. Under suitable conditions conductor can experience either aeolian vibration, galloping or wake-induced oscillation. Periodic vortex shedding causes aeolian vibration. Galloping is an aerodynamic instability, which can occur if the cross-section of a conductor is asymmetric, e.g., due to ice deposit. Wake-induced conductor vibration is restricted to bundled conductors. It is initiated when the leeward conductor is subjected to a complex force field created by the wake of the windward conductor. While galloping and wake-induced vibration are quite rare phenomena, aeolian vibration can be regarded to be almost always present.

The aim of this paper is to present results of studies made for the covered overhead line conductor LMF SAX 185. This conductor type is used in a 110 kV covered conductor line in western Finland, Fig. 1. Studies reported in this paper are focused on the aeolian vibration. It is shown how the energy (or power) balance method (Cigre SC22-WG01 1989, Cigre SC22-WG11 1998) is used to calculate the conductor lifetime. Two new formulations for self-damping power are presented and

[†] Product Development Manager

[‡] Research Engineer



Fig. 1 Studied 110 kV covered conductor line in western Finland

compared with two widely used empirical models using measured self-damping data. Finally, the calculated lifetime estimates are compared with those produced by field measurements. In addition, comparison with safe design tensions reported by Cigre (SC22-WG11 1999) is made.

2. Wind power input

In order to be able to use energy balance principle for calculating vibration amplitude one needs to know the power fed into the conductor by the wind. Wind power imparted to a conductor is normally determined by means of wind tunnel measurements. The wind power per conductor unit length P_w is normally calculated using following equation

$$P_w = f^3 d^4 \cdot WPF\left(\frac{Y}{d}\right) \quad (1)$$

where f is the vibration frequency, d is the outer diameter of the conductor, $WPF(\)$ is the empirical wind power function and Y is the single vibration amplitude (0-to-peak) at antinode.

Several studies concerning wind energy input to a conductor have been made and many empirical wind power functions have been developed. A summary of various wind power curves has been presented e.g., in Birka and Laneville (1996), and Kantola (2002). Vortex excitation is self-limiting, thus after the vibration amplitude has reached certain value the wind power fed into the conductor starts to decrease. In this study turbulent wind power functions given by Rawlins (1998) are used. Fig. 2 shows the value of $WPF(\)$ as function of normalised antinode amplitude for turbulence intensities 10-30%. The air density value of 1.293 kg/m^3 was used in the calculation of these curves.

The wind turbulence level has an impact on the wind power imparted to the conductor. The wind turbulence intensity is defined as

$$TI_z = \frac{\sigma_z}{V_{mz}} \quad (2)$$

where V_{mz} and σ_z are the mean wind velocity and the standard deviation of the wind speed at altitude z , respectively. Laminar wind flow produces the maximum wind power. Turbulence reduces wind power mainly due to span-wise variation of wind velocity and fluctuation of wind velocity with time. The wind turbulence intensity increases with ground roughness and decreases with

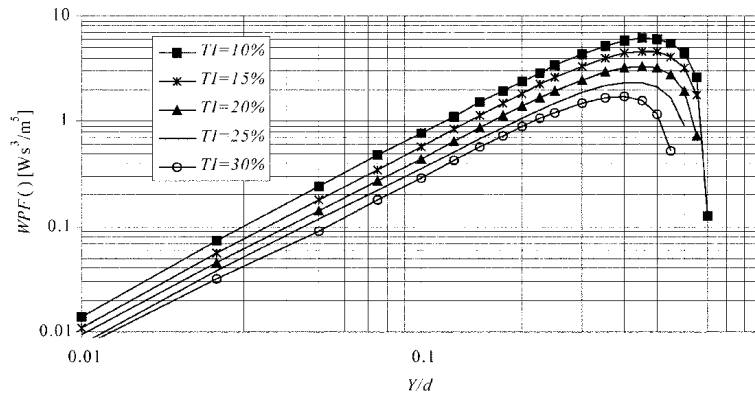


Fig. 2 Empirical wind power functions for turbulence intensities of 10-30%

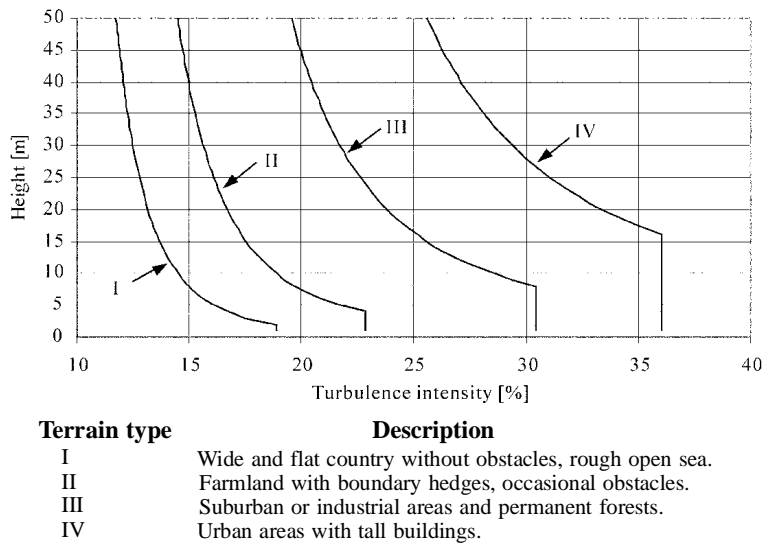


Fig. 3 Turbulence intensity curves (upper boundary) for different terrain types

altitude. Furthermore, the turbulence intensity normally decreases when the mean wind velocity increases. Turbulence intensity can be approximated if the terrain type and height above ground is known. Fig. 3 presents how turbulence intensity depends on terrain type and height above ground according to Eurocode 1 (European Committee for Standardisation 1995).

Terrain categories encountered along the studied overhead line are estimated to be type II and III (terrain type II in Fig. 1). The conductors are hanging between 8... 16 m above ground, so according to Fig. 3, the wind turbulence intensity level is expected to be roughly in the range of 15 ... 30%.

3. Conductor self-damping power

In addition to wind power fed into the conductor also the damping of the system (self-damping & external dampers) must be known in order to be able to calculate the steady-state vibration level by the concept of energy balance.

The self-damping characteristics depend on conductor type, tension, vibration amplitude, frequency or wavelength and temperature (covered conductors). The dependency is strongly non-linear. Self-damping is defined as the average power dissipated per unit length (during one cycle) of a conductor vibrating in a natural mode. Conductor self-damping consists of two main sources: material damping, i.e. energy dissipation in the material itself and system damping, mostly due to Coulomb friction, which causes energy loss when slip occurs between individual strands.

Due to the complexity of conductor self-damping, the only reliable way to determine it is to carry out measurements.

3.1. Self-damping measurement techniques

Self-damping measurement methods can be divided into two main groups, which are usually referred to as free vibration methods and forced vibration methods. Free vibration or decay methods are based on the fact that the rate of decay of a freely vibrating system is a function of the losses within the system. In the forced vibration methods, the shaker maintains the uniform steady-state amplitude by replacing the specimen losses.

3.1.1. Free vibration methods

In the free vibration methods there is no external excitation forces acting during measurements. The dissipation power is defined indirectly with the aid of measured damping coefficient. The damping coefficient can be estimated many ways, but mostly used method is based on logarithmic decrement. The logarithmic decrement approach supposes that one mode dominates the measured response. This means that continuous systems must be excited such a way that only the interesting mode dominates the free response. This requirement introduces severe difficulties in practical test setup. On the other hand, one measurement produces damping coefficients for a wide range of vibration amplitudes due to the decaying response.

The conductor must be excited into the damped natural frequency somehow and therefore, the measurement results can be greatly affected by the method used to disconnect the driving force. Suddenly released force generates an impulse to the conductor. Because an impulse has a wide frequency spectrum, other vibration modes will be excited as well, which may contaminate the measurements.

Although logarithmic decrement is a widely used concept in structural vibrations, there is one severe limitation concerning decrement methods when applied to conductors. Remarkable part of the conductor self-damping may be due to Coulomb friction, especially for bare conductors. Free vibration of a system having dry friction damping decays linearly rather than exponentially. Because the logarithmic decrement is unique, if and only if, the decay rate is exponential, it is questionable to apply decrement methods to conductors.

3.1.2. Forced vibration methods

The frequency of the excitation force is tuned to a desired undamped natural frequency. It is easy to verify that no other modes than the principal mode participate excessively to the operating mode shape^[1] under investigation by studying the resulting frequency (Fourier) spectra of the measured responses.

^[1]The operating mode shape is the true deflection or vibration shape. It is always a weighted sum of the mode shapes. Strictly speaking, a measured forced vibration mode is always an operating mode shape. The closer the excitation frequency is to the undamped natural frequency the closer the operating shape is to the true mode shape.

In the Inverse Standing Wave Method (ISWM), the self-damping power is measured for a particular loop. Consequently, ISWM does not produce averaged power dissipation over the whole test specimen, which may be an advantage as well as a disadvantage. ISWM is insensitive to the end losses at clamps, which is perhaps the most important feature in this method.

In the ISWM the fundamental quantities to be measured are the vibration amplitudes at two adjacent nodes, the maximum vibration amplitude on that loop and the corresponding loop length. In addition, the vibration frequency, conductor tension and the conductor mass per unit length are needed.

The estimated relative measurement error in self-damping power for ISWM is (Kantola 2002)

$$\varepsilon = \left| \frac{\Delta P_c}{P_c} \right| \approx 2 \left| \frac{\Delta s}{\pi \zeta} \right| \quad (3)$$

where it has been assumed that both inverse standing wave ratios $s (s = Y_{node}/Y)$ have been measured with the same accuracy Δs . This states that the absolute error in inverse standing wave ratio must be two decades smaller than the equivalent viscous damping ratio ζ of the conductor. For instance, if we assume that the relative viscous damping coefficient is 0.01% and we accept 5% error in self-damping power, the inverse standing wave ratio must be measured with six digits accuracy. One should note that measuring displacements accurately is very difficult in practice. Several researchers have noticed this problem (e.g., Diana *et al.* 2000). However, for heavily damped systems, for instance conductors with external damper, ISWM might be a good choice. The correct measurement requires accurate location of two nodes. It should be remembered that at nodes, the slope of a mode shape is at maximum and therefore, a small perturbation in location of the node may cause severe loss in accuracy. The problem can partly be corrected by measuring many points around a node (e.g., Diana *et al.* 2000). ISWM requires that displacements be measured using non-contacting sensor. Accelerometers cannot be used due to damping effect of the accelerometer cable, which can produce damping of same order than the conductor itself.

In the Power Method the power input into the system is determined directly from the excitation force, resulting acceleration (velocity or displacement) and the corresponding phase angle at the point of application of the load.

If a harmonic force is acting on the conductor at one undamped natural frequency f_n the average power dissipated per unit length during one period by the conductor of span L is

$$P_c = \frac{FA}{2L(2\pi f_n)} |\sin \phi| - P_0/L \text{ for measured Acceleration} \quad (4)$$

where F and A are the measured force and acceleration amplitudes, respectively. The shaker position is not necessarily located at antinode. P_0 is the total power dissipated at span ends and it should be measured separately. Whenever the stiffness of the span termination is high enough, end span damping P_0 is mostly due to structural damping within the conductor in a narrow region near clamps where the conductor is forced to bend severely. If the span length L is long enough, the power dissipated near the clamps is small in comparison to the conductor self-damping.

Eq. (4) is based on the assumption that both the excitation force and the response are simple harmonics. If amplitudes and phase angle ϕ are defined from Fourier spectra, this is always the case and P_c is therefore the power dissipated at the desired natural frequency f_n neglecting the contribution of all the other frequency components. The force and response product can be estimated easily from the measured cross-spectrum, because $FA \sin \phi$ is equal to the imaginary part of cross-spectrum between the force and acceleration.

The estimated relative measurement error in self-damping power for power method is (Kantola 2002)

$$\varepsilon = \left| \frac{\Delta P_c}{P_c} \right| \approx \left| \frac{\Delta F}{F} \right| + \left| \frac{P_0}{LP_c} \right| \quad (5)$$

The error estimate is valid for odd-numbered modes, if the exciter is attached at the mid-span (where anti-nodes of all the odd-numbered modes are located). When the exciter is not located at the mid-span, the relative error in acceleration must be added to the error estimate. Because the force (and acceleration) can be measured extremely accurately using piezoelectric transducers, it is clear that power method introduces measurement errors several times smaller to that of ISWM.

3.2. Practical test arrangement for power method

Test arrangement used in this study is shown in Fig. 4.

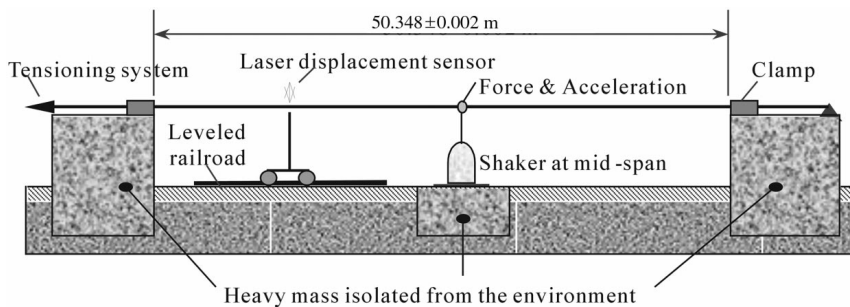


Fig. 4 The test arrangement used in this study (NK Cables, Finland)

The tension apparatus is an inverter controlled electric motor driven screw, which automatically adjusts the tension to a desired value. The termination clamp bolts were tightened according to a pre-defined procedure, which guaranteed that the final conductor tension remained very close to that set by the screw. The stiffness of the termination clamps was measured by exciting the conductor at mid-span position and by measuring the transmissibility from the driving point to the clamps. In the frequency range from 0 through 160 Hz, the transmissibility was less than 0.1% at all frequencies, indicating that the clamps were stiff enough. The end clamps have been designed in such a way that they should not raise the measured damping values.

The shaker and the laser sensor were set on a “railroad” of length longer than the half-span, which made it easy to change their places along the cable. This was needed, because the location of the maximum loop amplitude measured with the laser sensor varied from mode to mode^[2].

The excitation force is fed to the conductor via a special extremely low-damped rod system, which is flexible (soft) in all directions in order to avoid excessive shear force and bending moment about the force cell. The rod is soft also in the excitation direction reducing distortion in the force signal and the mode shape. The force is measured by means of piezoelectric load cell, which was located on the top of the rod and the flexible device in order to reduce inertia forces. The total extra or added mass above the load cell is about 20 grams. In order to check the effect of the added mass

^[2]To be precise, the maximum loop amplitude was taken as the maximum got from the laser sensor and the acceleration at shaker position.

on the measurement results, additional extra masses were installed above the load cell: no changes in damping power were recorded. Excitation rod is electrically insulated from the conductor in order to avoid ground loops.

3.2.1. About practical power method measurements

Although the practical measurements seem to be easy to perform, there are some aspects, which should be recognised. The test must be performed in stable environmental conditions. Authors' experience is that by opening loading doors of a large industrial hall may destroy the measurements due to temperature changes and/or air blast, although the doors were as far away as 100 meters from the test site.

The resonant frequency differs from the undamped natural frequency at which the conservative forces cancel out ($m\ddot{y} + kx = 0$). It is therefore not possible to tune an arbitrary system at undamped natural frequency by maximising the response. The correct method to achieve undamped natural frequency irrespective of the damping model is to tune the phase angle between force and response to zero (for velocity) or ± 90 degrees (for displacement and acceleration). Because the conductor self-damping is typically very low, the phase angle between the driving point force and acceleration changes very rapidly around the undamped natural frequency. Therefore, very fine frequency accuracy is needed which states heavy requirements to the function generator. The sine generator used in this study had frequency accuracy of 1 μ Hz.

Elliptical motion takes place if both the vertical and transverse natural frequencies are close enough to the excitation frequency. This happens due to the conductors' stranded structure, although the excitation force is exactly vertical. Large transverse loads may be generated to the load cell disturbing the force measurement due to the bending moment and shear force, although the excitation rod were soft in transverse direction. If elliptical motion was noticed, the measurements associated to this particular mode were discarded.

A kind of dynamic ageing procedure was applied to the conductor, because old vibrated conductors have a slightly lower self-damping than new conductors.

The force and response signals were recorded using an advanced spectrum analyser. Flat-Top weighting window was used in order to obtain the most accurate amplitude value at the desired frequency component, an error estimate being less than 0.1%. Flat-Top window can be utilised, if the adjacent modes do not affect on the amplitude of the desired mode. Note that in this study the exciter was placed at mid-span, which effectively doubles the frequency band between adjacent modes.

3.3. Pre-processing of the measured data

During the measurements, the tension force T may vary in respect to time due to temperature changes. Conductor's temperature may be altered due to the environmental temperature variations and due to dissipation energy during the measurements. Temperature variations can be compensated using a method based on curve-fit of the measured natural frequencies f_n

$$f_n^2 = C_2(b_n L)^2 + C_4(b_n L)^4$$

$$C_2 = \frac{T/m}{(2\pi L)^2} \quad C_4 = \frac{EI/m}{(2\pi L^2)^2} \quad (6)$$

where m is the conductor mass per unit length and $b_n L$ is the solution of the associated characteristic equation (rigidly supported conductor)

$$\tan b_n L \approx b_n L \sqrt{4 \frac{EI}{TL^2}} \sqrt{1 + (b_n L)^2 \frac{EI}{TL^2}} \quad (7)$$

Once the coefficients C are known, the true average tension T and the dynamic average bending stiffness EI during the measurements can be extracted as

$$T = C_2 m (2\pi L)^2, \quad EI = C_4 m (2\pi L^2)^2 \quad (8)$$

The solution of C coefficients is iterative, because the roots of the characteristic equation are not known a priori. It can be assumed that Eqs. (8) are very accurate, because the natural frequencies are normally measured with very high accuracy. It should be emphasised that T and EI approximated in this way are the effective values which give the most accurate analytical natural frequencies in respect to the measured natural frequencies in least squares sense.

Curve-fitting natural frequencies gives a new set of natural frequencies associated to the average tension and bending stiffness during the tests. In addition, the fitted natural frequencies satisfy the characteristic equation exactly. It can be concluded that the fitted natural frequencies, calculated average tension and bending stiffness form a consistent conductor database in conjunction with L and m . Therefore, a measurer should consider using calculated values for tension T and natural frequencies f_n instead of measured ones when fitting measured data into empirical models (as done in this study).

3.4. Effect of aerodynamic damping

Because the self-damping test is performed in still air, the measured self-damping is the sum of aerodynamic fluid damping and conductor self-damping. In practice, the conductor vibrates in such conditions where there is no aerodynamic damping present or it is small. Therefore, aerodynamic damping must be subtracted from the measured damping. There is no ‘‘absolutely correct’’ mathematical expression for the aerodynamic damping. In this study, perhaps the most widely used formula, the modified Sarpakaya’s equation (Noiseaux *et al.* 1986).

$$P_a = \frac{\pi}{16} \left[\frac{4\sqrt{2}}{\sqrt{Re}} + 0.65 \left(\frac{Y}{d} \right)^2 \right] \rho_a (2\pi f_n)^3 d^2 Y^2 \quad Y/d < 1.6, \quad Re < 10,000 \quad (9)$$

was utilised. ρ_a is the air density and Re is the Reynolds number, defined as $Re = \rho_a (2\pi f_n) d^2 / \mu_a$ where μ_a is the air viscosity. The net or true self-damping power is then

$$P_d = P_c - P_a \quad (10)$$

3.5. Empirical models for conductor self-damping power

In order to make future calculations easier it is advantageous to fit an appropriate formula to measured data. The following four formulae for the average Self-Damping Power Functions, $SDPF$, per unit length (Kantola 2002)

$$\begin{aligned}
\frac{P_d}{f_n Y^2} &= a T^{-b} Y^c \bar{f}_n^{-d} && \text{Original Cigre} \\
\frac{P_d}{f_n Y^2} &= a T^{-b} Y^c \lambda_n^{-d} && \text{Original Claren} \\
\frac{P_d}{f_n Y^2} &= a(1 + \alpha_Y Y^2)(1 + \alpha_V \bar{f}_n f_n Y) \cdot T^{-b} Y^c \bar{f}_n^{-d} && \text{Modified Cigre} \\
\frac{P_d}{f_n Y^2} &= a(1 + \alpha_Y Y^2)(1 + \alpha_V \bar{f}_n f_n Y) \cdot T^{-b} Y^c \lambda_n^{-d} && \text{Modified Claren} \quad (11)
\end{aligned}$$

will be compared. There are also other formulations, for instance those based on curvature of the vibrating cable (Rawlins 2000). The ‘conductor-type’ constants a and all the exponents are not necessarily equal from equation to equation. In the right-hand side it is advantageous to use the taut string corrected frequency

$$\bar{f}_n = f_n \sqrt{\frac{m}{T}} \quad \bar{f}_n = \lambda_n^{-1}, \quad \text{if } EI = 0 \quad (12)$$

instead of natural frequency. Although, not relevant in theory, this replacement reduces numerical value of the tension exponent significantly.

In the modified expressions, the first term in round brackets accounts for the effect of conductor length variation due to vibration; this is important especially for material damping of conductor sheath. Second term in round brackets is the first order extension of the classical non-linear viscous damping model. This additional term is expected to be related to the first power of vibration velocity ($\propto f_n Y$) and its coefficient is assumed to depend linearly on the taut string corrected frequency.

Models based on Cigre are the most pragmatic representations, because they use the primary measurement variables (Y and f_n) from laboratory tests and therefore, any conversion from frequency to loop length is not needed. Measuring the loop length accurately is not a simple task, because the loop length differs somewhat from loop to loop and the definition of the nodes is very time consuming. Furthermore, if the system has complex vibration shapes the nodal points do not have fixed locations but change places as a function of time. Therefore, it is recommended to approximate the loop length mathematically for the models based on Claren (Kantola 2002).

It should be noted that all the empirical models can account material damping (metal and plastic) and interface slippage damping, if one of these mechanisms dominates. In general, none of these models are correct if both mechanisms are meaningful. It is difficult to say which one of the self-damping power equations would be best for a particular conductor. Therefore, it is best to curve-fit all of them. Appropriate error parameters should be calculated in order to rank the models.

3.5.1. About mathematical solution of model parameters

Large discrepancies in the measured self-damping parameters of identical conductors, strung at the same tension, have been reported. Problem formulation and the solution algorithm selection may be

one reason for these discrepancies, because there might be several almost equal good solutions, especially if the problem is ill-conditioned or too few measurements have been done. Therefore, the mathematical formulation needs attention when measured data is in question. Because the system is normally highly over-determined, i.e., there are much more equations than unknowns, it must be solved by minimising an appropriate penalty function. Perhaps, the fundamental question is, should we minimise relative or absolute errors in the model. Data weighting may also be an important aspect.

3.5.2. Comparison of the empirical models

In this section, empirical models will be compared for the LMF SAX 185 conductor. Measurements have been performed using three different tensions (7,470, 9,350 and 11,160 N) and three different velocity levels (70, 140 and 210 mm/s) at frequency range from 11 Hz through 65 Hz. The aerodynamic damping power was subtracted from measured self-damping power using Eq. (9). The total number of measurements was about 100. The solutions have been found using Microsoft® Excel Solver add-in by minimising the relative error between the model and measured data rather than absolute error.

The performance of the original formulations has been presented in Fig. 5. The left-hand side figures illustrate the model accuracy in ‘measured data - modelled data’ axes. The bold straight line

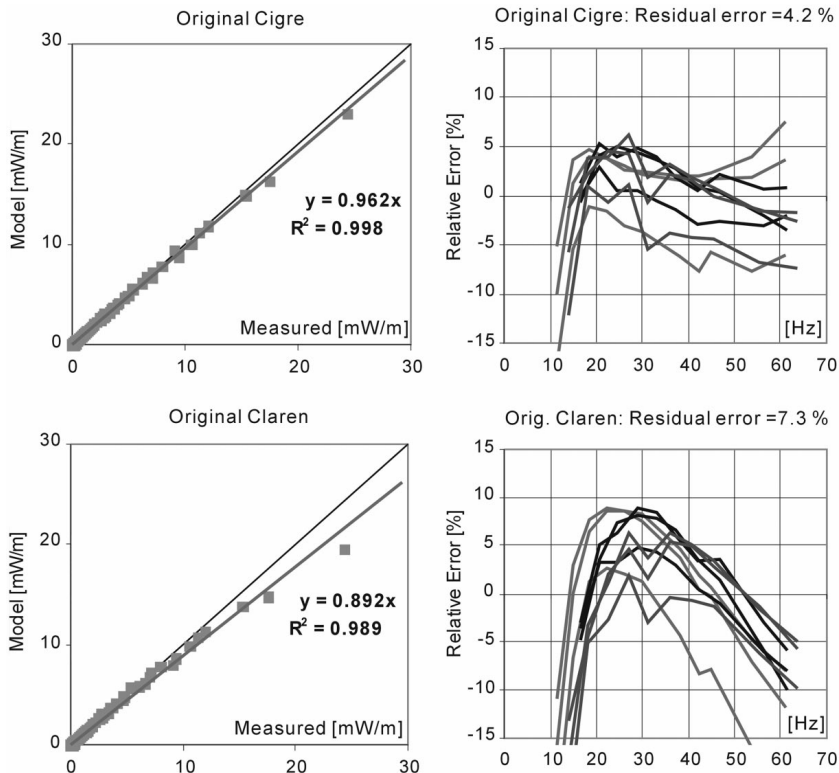


Fig. 5 Performance of the original formulations by Cigre and Claren

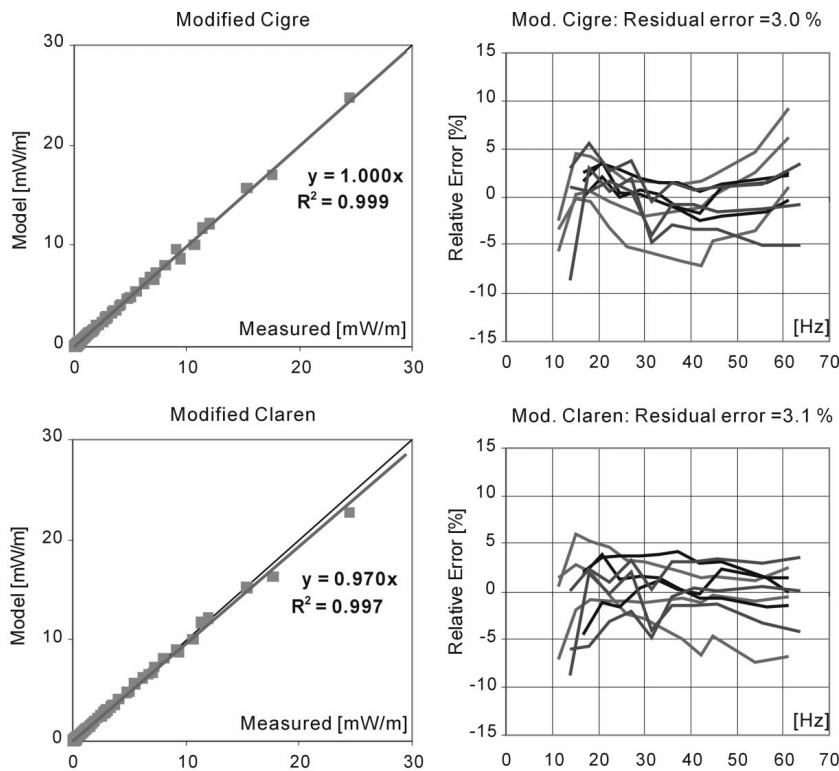


Fig. 6 Performance of the modified empirical models

Table 1 Model parameters for LMF SAX 185 covered conductor

	a	b	c	d	α_y	α_v
Cigre	15.153	0.123	0.164	3.771		
Claren	127.19	0.301	0.158	4.046		
M. Cigre	12.646	0.154	0.006	3.563	0.03790	0.01769
M. Claren	28.946	0.586	-0.714	2.386	0.07305	0.65578

is the best linear fit between the measured and modelled data: the slope of this line should be unity. If the slope is unity, the model represents the measured data correctly in average. This is, however, not enough, because the data points may still fluctuate remarkably around the average. The correlation coefficient squared R^2 is one measure for that, and it should also be unity. Unfortunately, the correlation coefficient is not very good measure for deciding whether an observed correlation is statistically significant, and/or whether an observed correlation is significantly stronger than another (Press *et al.* 1988). Therefore, the right-hand side figures show the relative error between the measured and modelled data. It is not necessary that these errors are zero, much more important is that errors do not tend to grow at any frequency. The residual error is the average relative error between the measured and modelled data: the smaller the better, if the relative error curves behave evenly.

The results of the modified empirical models are presented in Fig. 6.

Table 1 shows results obtained for the studied conductor. The single vibration amplitude Y is

expressed in millimetres. The resulting self-damping power has unit of mW/m.

Due to the best performance of the modified Cigre model, it was selected to be used in Energy Balance calculations described in the next section.

4. Estimated conductor lifetime

The Energy Balance Principle is an analytical method of estimating the aeolian vibration level. The basic idea is to find the steady-state vibration amplitude level at which the wind power fed to the conductor equals the conductor net damping power:

$$P_w = P_d \quad (13)$$

4.1. Estimation of vibration amplitudes

The bending stiffness (EI) of a conductor must be known in order to convert estimated vibration amplitudes into the maximum stress values. The bending stiffness can be measured for the desired tensions, but for lifetime estimation, calculated values may be accurate enough.

For a tensioned conductor two extreme values can be calculated. If it is assumed that the strands act independently, i.e., they are not bound together and have therefore a gliding contact, the minimum value for moment of inertia (I_{\min}) is obtained. The maximum value (I_{\max}) is obtained if the strands are assumed to be “welded” together, i.e., no slippage between the strands occurs. Because the phenomenon is related to strand slippage or inter-strand motion within a conductor, it appears that I varies with conductor deformation, meaning that it is not constant along a vibrating conductor, and varies with time during the vibration cycle. This means that when estimating the conductor strain in the outer lay close to a rigidly supported clamp, I_{\min} should be close to the true value. However, in estimation of loop lengths, natural frequencies or any other global properties the true moment of inertia, according to experiments, is about one-half of I_{\max} . This is most probably true for an uncovered conductor. For a conductor with thick sheath, no inter-strand slippage necessarily takes place, and the calculated maximum bending stiffness is closer to the true global average bending stiffness. For the studied covered conductor the measured global average EI (extracted from Eq. (8)) is practically equal to the calculated EI_{\max} .

In order to obtain the maximum vibration amplitude Y over the whole vibration frequency band Eq. (13) is solved for the frequencies of interest. Fig. 7 shows the result of the EBA made for the studied conductor. In the calculation turbulence intensity value of 15% was used. The conductor was tensioned to 7,440 N. The bending stress amplitudes have been calculated as follows:

$$\sigma_{\max} = \pi Y f_n \sqrt{\frac{m}{EI_{\min}}} \cdot E_a d_a \quad (14)$$

d_a and E_a are the diameter and the modulus of elasticity of an outer layer strand, respectively.

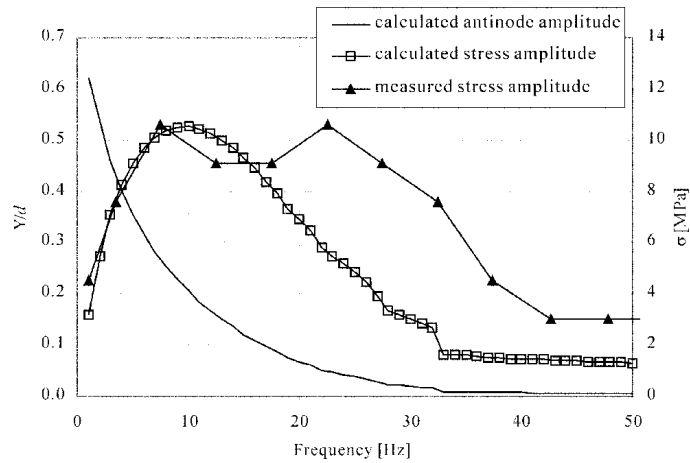


Fig. 7 Normalised antinode amplitude (Y/d) and stress amplitude σ of a conductor wire derived from EBA ($TI=15\%$, $T=7440$ N). Measured stress amplitudes (Span 7-8, Measurement Period I) c.f. Section 5

4.2. Calculation of number of cycles

The conductor vibrates at a frequency given by Strouhal law:

$$f = St \frac{V_w}{d} \quad (15)$$

where St is the Strouhal number (≈ 0.185) and V_w is the wind velocity perpendicular to the conductor. Consequently, if one knows the wind velocity distribution near the line one can approximate the vibration frequency distribution and furthermore the number of vibration cycles within a specified time period, e.g., a year.

Aeolian conductor vibration can be categorised as a narrow frequency band of random vibrations (Noiseux, Hardy and Houle 1987). This is due to the fact that a given wind velocity excites only a small number of natural frequencies. The probability distribution of the amplitudes and stresses of a narrow-band Gaussian random process is approximately equal to the Rayleigh distribution

$$p(\sigma) = \frac{\bar{\sigma}}{\sigma_{\text{rms}}} e^{-0.5\bar{\sigma}^2} \quad \bar{\sigma} = \frac{\sigma}{\sigma_{\text{rms}}} \geq 0 \quad (16)$$

The maximum bending stresses obtained from Eq. (14) can be transformed to rms-values by using the peak factor approach (Leskinen 1998, Eurocode 1), or simply assuming that $\sigma_{\text{rms}} = \sigma_{\text{max}}/3$ taking into account that on average only about 1% of the maximum values exceed 3 times the rms-value (Newland 1989).

Knowing now the frequency and stress distributions one can calculate the number of cycles for each frequency-stress -pair. Fig. 8 shows calculated number of vibration cycles n within a year for the studied conductor as function of vibration frequency and stress amplitude. The wind velocity distribution of the nearby weather station was used in the analysis. The wind directional preferences and vibration build-up time has been taken into account by using a method showed in Leskinen

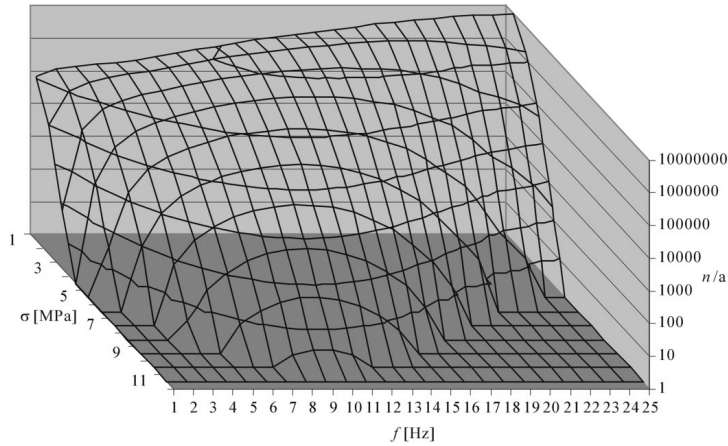


Fig. 8 Calculated number of stress cycles within a year

(1998). Fig. 8 demonstrates that the number of high stress cycles is very small in comparison to low stress level cycles.

4.3. Lifetime estimates

Conductor lifetime can be estimated by using Palmgren-Miner rule

$$\sum \frac{n_i}{N_i} = 1.0 \tag{17}$$

where N_i denotes the allowed number of cycles obtained from the S-N curve at stress level i . In this study the S-N curve given in (Cigre SC22-WG4 1979) is used. The Cigre safe borderline is a conservative S-N curve based on fatigue tests of different conductor types. Fig. 9 presents the S-N curve and the accumulated stress cycles calculated for a period of one year for the studied case.

Repeating lifetime calculations for different conductor tensions and wind turbulence intensities (terrain types) one gets a graph like in Fig. 10. This type of figure helps the line designer to choose the right conductor tension for different terrain types. The lifetime of the studied conductor is proportional to $T^{-8} \cdot TI^{3.5}$.

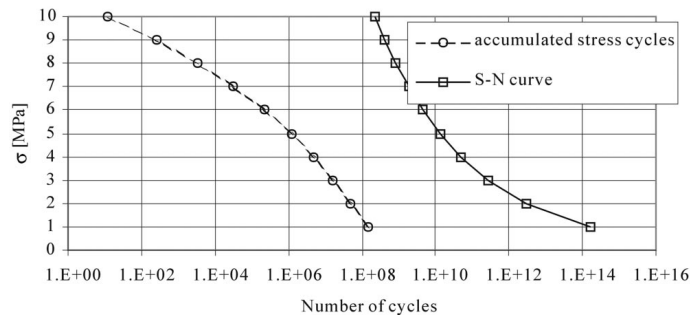


Fig. 9 Accumulated stress and S-N curves

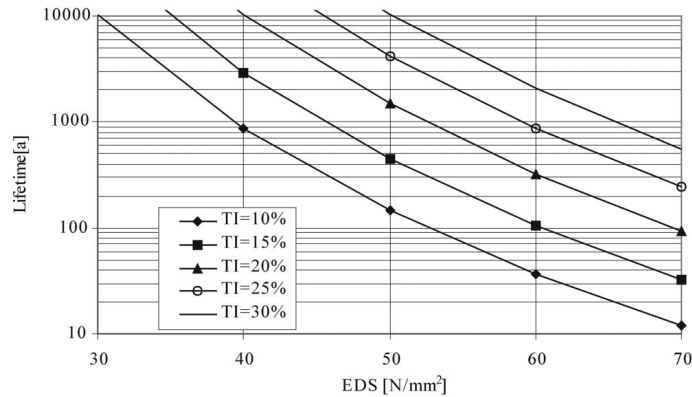


Fig. 10 Conductor lifetime estimates as function of turbulence intensity and conductor tension expressed as tension stress at 0°C

5. Field measurements

Conductor vibration measurements were conducted on the studied overhead line. The measurement procedure followed the guidelines given in (Cigre SC22-WG11 1995). In the field measurements the bending amplitude Y_b , the vibration frequency and the number of cycles for each amplitude-frequency pair was recorded. In the studied overhead line, AGS-clamps were used for the conductor suspension (c.f. Fig. 11).

Measured bending amplitudes Y_b (peak-to-peak) were converted to stress amplitudes σ_b (0-to-peak) using Poffenberger-Swart formula

$$\sigma_b = \frac{E_a d_a p^2}{4(e^{-px} - 1 + px)} Y_b \quad p^2 = \frac{T}{EI_{\min}} \quad (18)$$

where x is the distance from the last point of contact between the conductor and the suspension clamp to the probe. For normal clamps the standard value of x is 89 mm. Due to the cage area of



Fig. 11 Vibration recorder installed below AGS-clamp

the AGS-clamp the measurement point had to be moved to a point 250 mm from the centre of the clamp. In the previous measurements (Leskinen 1998) it was found that Poffenberger-Swart formula does not give accurate results with AGS-clamps. The right-hand side of the Eq. (18) has to be multiplied by factor of 2.2 in order to give results comparable with strain gauge measurements.

The field vibration measurements were performed in four spans. The two spans between poles 7-8-9 were in the middle of farmland area where relatively low turbulence intensity levels (10...20%) were expected (c.f. Figs. 1 and 11). The spans between poles 40-41-42 were situated in a more shielded area where turbulence intensity values were expected to be in the range of 20...30%.

6. Comparison between EBA and field measurement results

Cigre's S-N curve was used in lifetime analysis of both methods. Table 2 summarises the results of these analyses.

Table 2 shows that EBA gives generally lower lifetime estimates in comparison with field measurements. This can be explained partly by the additional damping existing in conductor suspension point not taken into account by EBA. Furthermore, the true turbulence intensities might differ somewhat from the assumed ones; this can either reduce or extend the lifetime.

In Fig. 7 the measured and the calculated stress amplitudes are compared. The comparison is made for span 7-8, measurement period I, where the measured lifetime estimate is less than calculated one. It can be seen that maximum stress amplitudes are about of same level, but measured stress amplitudes are larger for wider frequency band. This indicates paradoxically that there is less damping at higher frequencies in true system or the higher wind velocities are able to feed more power to the conductor than expected.

One of the recorders measured wind velocity perpendicular to the line. The measured wind velocities (averaging time was one second) were linked to the measured amplitude-frequency pair. This data was used to verify that Strouhal law (Eq. (15)) is valid.

Fig. 12 compares the measured and calculated Strouhal frequencies according to Eq. (15). Figure shows that for higher wind velocities measured frequencies are too low compared to calculated frequencies with a Strouhal number value of 0.185. The one-second averaging period can explain this discrepancy, because it enables the recording of wind gusts. These wind gusts do not normally affect aeolian vibration due to lock-in phenomenon and their short duration.

Table 2 Lifetime estimates based on field measurements and EBA

Measurement period			I		II	
Start date			2000-01-20		2000-04-27	
End date			2000-04-27		2000-08-03	
Span (poles)	Length [m]	TI [%]	Lifetime [a]		Lifetime [a]	
			Measured	EBA	Measured	EBA
7-8	138	15	1300	2195	10743	4906
8-9	134	15	9931	2195	115199	4906
40-41	137	25	44372	21858	114432	47033
41-42	150	30	468626	55688	572205	120638
Mean temperature			-0.8°C		+13.1°C	

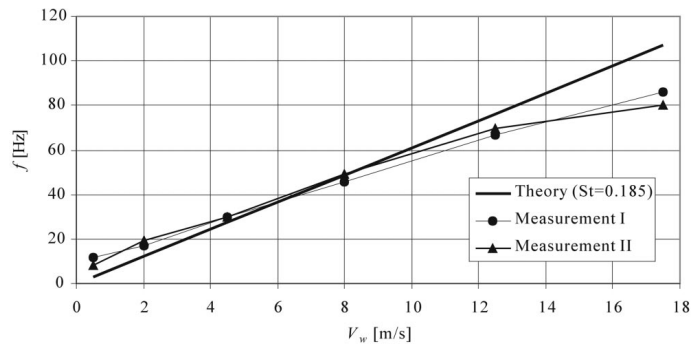


Fig. 12 Measured vs. theoretical Strouhal frequencies

7. Safe design tension

Cigre (Cigre SC-22 WG11 1999) has published a report concerning safe design tensions with respect to aeolian vibration. In this report safe design tensions are given by means of the parameter H/w , where H is the conductor tension [N] at the average temperature of the coldest month and w is the conductor weight per unit length [N/m]. Furthermore, the terrain type where the overhead line is situated has influence on the safe design tension: in open flat terrain types lower conductor tension has to be used in order to avoid wire fatigue. According to the report allowable H/w - parameter value for terrain category 3, which is described as “open, flat, or undulating with very few obstacles, e.g., open grass or farmland with few trees, hedgerows and other barriers; prairie, tundra”, is 1225 m.

The studied line is situated near the town of Pori, where the average temperature of the coldest month is -6.6°C (1961-1990). For the LMF SAX 185 -conductor with EDS of 40 MPa (ruling span 140 m) this leads to H/w value 785 m, which is on the safe side even for the terrain type 1 ($H/w = 1000$).

8. Conclusions

It is concluded that the power method gives the most reliable self-damping results among the available techniques. The conductor tension may vary during the test causing inaccuracies when the measured data is curve-fitted into empirical models. The presented new pre-processing method reduces these errors. Data pre-processing produces a new set of natural frequencies associated to the average tension and bending stiffness during the tests. In addition, the pre-processed data satisfies the characteristic equation exactly.

Cigre’s and Claren’s well-known empirical models were enhanced to increase their performance especially at low and high frequencies. It was noticed that both modified formulations do a better job than the original models.

Both energy balance analysis and field measurements give satisfactory lifetime estimates for the studied conductor. This is also in agreement with the recommendations for the safe conductor design tensions.

The fact that EBA generally gives lower lifetime estimates than field measurements can be

explained partly by the additional damping produced by the suspension system, which is not taken into account in EBA. Furthermore it should be noted that EBA leads to long-term results and should thus give conservative result in comparison to short-term field measurements.

The field measurements were performed in two periods, whose mean temperatures differ ca. 14°C. The results of the second measurement period suggest greater lifetime expectancy than the first one. This rise is mainly due to increased conductor damping, which is caused by higher damping of the conductor sheath and by lower conductor tension due to higher ambient temperature.

References

- Cigre Study Committee 22-Working Group 01 (1989), "Report on aeolian vibration", *Electra*, (124), 41-77.
- Cigre Study Committee 22-Working Group 4 (1979), "Recommendations for the evaluation of the lifetime of transmission line conductors", *Electra*, (63), 103-145.
- Cigre Study Committee 22-Working Group 11 Task Force 2 (1995), "Guide to vibration measurements on overhead lines", *Electra*, (163), 125-137.
- Cigre Study Committee 22-Working Group 11 Task Force 1 (1998), "Modelling of aeolian vibration of single conductors: assessment of the technology", *Electra*, (181), 53-69.
- Cigre Study Committee 22-Working Group 11 Task Force 4 (1999), "Safe design tensions with respect to aeolian vibration. Part 1: Single unprotected conductors", *Electra*, (186), 53-67.
- Brika, D. and Laneville, A. (1996), "A laboratory investigation of the aeolian power imparted to a conductor using a flexible circular cylinder", *IEEE Transactions on Power Delivery*, **11**(2), 1145-1152.
- Diana, G., Falco, M., Cigada, A., and Manenti, A. (2000), "On the measurement of overhead transmission lines conductor self-damping", *IEEE Transactions on Power Delivery*, **15**(1), 285-292.
- European Committee for Standardisation (1995), "Eurocode 1 (ENV-1991-2-4): Basis of design and actions on structures - Part 2-4: Actions on structures - Wind actions".
- Kantola, K. (2002), "Aeolian vibrations in single overhead conductors", Technical report for NK Cables Ltd, Helsinki University of Technology, Finland.
- Leskinen, T. (1998), "Wind-induced transmission line conductor vibration: theory and measurements", Licentiate thesis, Lappeenranta University of Technology, Finland.
- Newland, D.E. (1989), *An Introduction to Random Vibrations and Spectral Analysis*, 2nd ed. Longman Scientific & Technical, Essex, England.
- Noiseux, D.U., Houle, S., and Beauchemin, R. (1986), "Study of effective aeolian wind power imparted to single conductor spans", CEA project 146 T 328.
- Noiseux, D.U., Hardy, C., and Houle, S. (1987), "Statistical methods applied to aeolian vibrations of overhead conductors", *Journal of Sound and Vibration*, **113**(2), 245-255.
- Press, W.H., Flannery, B.P., Teukolsky, S.A., and Vetterling, W.T. (1988), *Numerical Recipes*, Cambridge University Press, NY.
- Rawlins, C.B. (1998), "Model of power imparted by turbulent wind to vibrating conductor", Alcoa Conductor products company, Technical note no. 31.
- Rawlins, C.B. (2000), "The long span problem in the analysis of conductor vibration damping", *IEEE Transactions on Power Delivery*, **15**(2), 770-776.